Carbonate content control in carbonate apatite coatings of biodegradable magnesium

Kazuma Midorikawa[a,b,c], Sachiko Hiromoto[a,b*] and Tomoyuki Yamamoto[b,d]

[a] *Research Center for Structural Materials, National Institute for Materials Science, Tsukuba 305-0047, Japan*

[b] *Faculty of Science and Engineering, Waseda University, Tokyo, 169-8555, Japan*

c *Present Affiliation: Nippon Steel Corporation*

[d] *Kagami Memorial Research Institute for Materials Science and Technology, Tokyo 169-0051, Japan*

* Corresponding author: Sachiko Hiromoto

(hiromoto.sachiko@nims.go.jp, 1-2-1 Sengen, Tsukuba, 305-0047, Japan)

Graphical Abstract

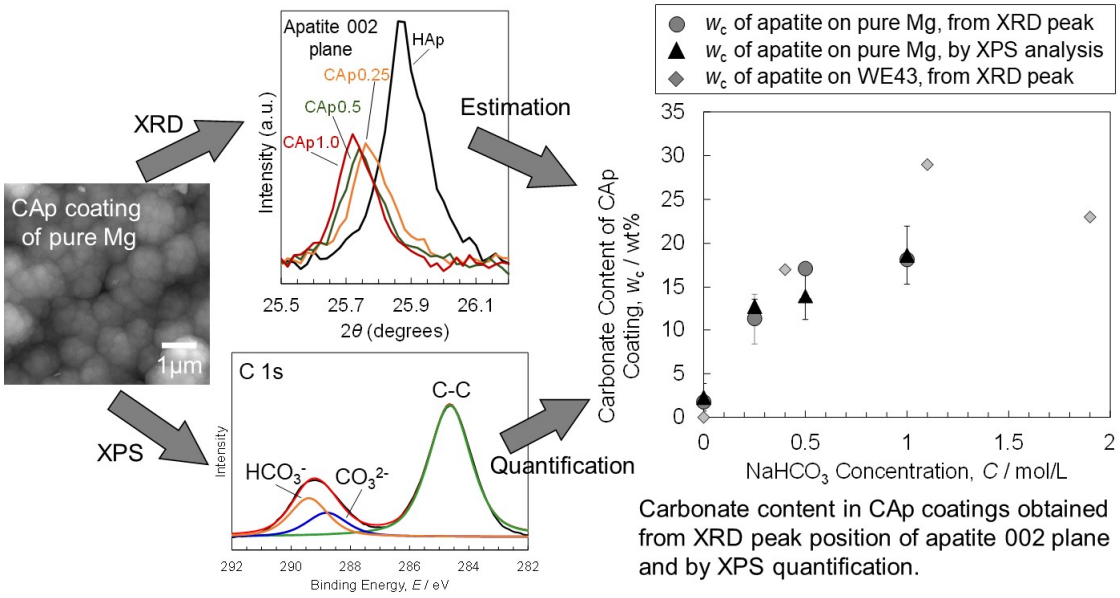

Carbonate content in CAp coatings obtained from XRD peak position of apatite 002 plane and by XPS quantification.

Highlights

- Variation of carbonate content of CAp coatings of pure Mg with $NaHCO_3$ concentrations
- Accordance in carbonate content derived from XRD peak position and XPS quantification
- Simple determination of carbon content of CAp coatings by XRD is possible
- Two types of carbonate group in CAp coatings, CO_3^{2-} and HCO_3^-

Abstract

Carbonate apatite (CAp) coating has been developed as a bioabsorbable corrosion-control coating for biodegradable Mg alloys. Carbonate content in the CAp coatings can be utilized to control the bioabsorbability and corrosion rate of CAp-coated Mg alloys. In this study, the carbonate content in the CAp coatings of pure Mg was varied by $NaHCO_3$ concentration of the coating solution from 0.25 to 1.0 mol/L, and hydroxyapatite (HAp) was formed without $NaHCO_3$. The CAp and HAp coatings were characterized using X-ray diffraction (XRD), X-ray photoelectron spectroscopy (XPS) and Fourier transform infrared spectroscopy (FTIR). The carbonate content in the apatite coatings formed with 0, 0.25, 0.5 and 1.0 mol/L $NaHCO_3$ was determined to be 2, 12, 15 and 18wt%, respectively, from the apatite 002 plane XRD peak position using the existing conversion constant as well as from the coating composition obtained by the XPS analysis. The values of carbonate content obtained by each method were in good accordance, indicating that the carbonate content can be determined simply by XRD measurements. Two types of carbonate group were present in the CAp coatings, CO_3^{2-} and HCO_3^-, and the relative content of HCO_3^- to CO_3^{2-} increased with an increase in the carbonate content.

Keywords: Carbonate apatite, Biodegradable magnesium, Coatings, Carbonate content, X-ray photoelectron spectroscopy, X-ray diffraction

1. Introduction

Magnesium (Mg) and its alloys have been extensively studied as a biodegradable material for biomedical applications, such as bone screws and plates and stents, because Mg is a biological essential element and Mg/Mg alloys show higher strength than biodegradable polymeric materials [1-5]. However, Mg/Mg alloys sometimes undergo unexpectedly rapid initial corrosion, which leads to the loss of strength and the rapid hydrogen gas generation to form gas cavities [6-9]. To overcome this issue, various surface modifications such as magnesium fluoride, calcium phosphate compounds and micro-arc oxidation (MAO) coatings have been developed to reduce the corrosion rate of Mg/Mg alloys while maintaining its biocompatibility [3, 10-18]. Among these, amorphous calcium phosphate, dicalcium phosphate dihydrate, β-tricalcium phosphate (β-TCP) and apatite coatings have been extensively developed owing to the excellent biocompatibility and bone conductivity, and these calcium phosphate coatings suppressed the corrosion of Mg/Mg alloys in vitro and in vivo [3, 10-16, 18-20]. The apatite and β-TCP coatings of Mg suppressed the pH increase of simulated body fluid (SBF) and Hanks' solution for about 5 days and 2 weeks, respectively, whereas the pH of these solutions increased rapidly from immediately after the immersion of uncoated Mg [19, 20]. Cheng et al. reported that $Mg(OH)_2$, MgF_2 and hydroxyapatite (HAp) coatings suppressed the gas accumulation around the samples implanted under skin of SD rat, and the HAp coating showed better osseointegration ability than the other coatings in rat femur [14].

We have developed HAp coatings [21-25], because HAp is used as artificial bone and bone conductive coatings of Ti alloy implants [26]. In the in vivo experiments, the HAp coatings retarded the corrosion of Mg alloys and enhanced the bone formation, while the HAp coatings were not absorbed in the surrounding tissue and the corrosion progressed

under the coating [22, 25]. HAp is stabile in physiological environments, as indicated by the fact that sintered HAp is not replaced with bone by osteoclastic resorption (degradation by osteoclasts) [27-30].

On the other hand, carbonate apatite (carbonate-substituted apatite) (CAp) can be replaced with bone by osteoclastic resorption. CAp is an apatite in which part of the phosphate and/or hydroxy groups are substituted by carbonate groups similar to bone apatite which contains 7.4-20wt% carbonate groups [28, 31, 32]: CAp with hydroxyl groups substituted by carbonate groups is referred to as type A and that with phosphate groups substituted as type B. Therefore, CAp coatings should be suitable for a bioabsorbable coating to provide a material in which both the coating and the substrate material are absorbed by the body. It has been reported that CAp is deposited to form a layer on Ti/Ti alloys and bioactive glasses by immersing in Kokubo's simulated body fluid (SBF) [33-36] and that the CAp layer formed on Ti-6Al-4V alloy is calcined under skin of Wister rat [36]. In the case of pure Mg, the SBF immersion led to the formation of very low crystalline apatite containing magnesium [11]. In the SBF immersion method, it is thus difficult to control the composition and structure of the apatite layers due to Mg ions released by the corrosion of the substrate Mg/Mg alloys. Then, a B-type CAp coating was developed by modifying our HAp coating method in which $NaHCO_3$ was added to the HAp coating solution, using Mg-4mass% Y and 3mass% rare earth (WE43) [37, 38]. Cell culture tests exhibited that the developed CAp coating can be absorbed by osteoclasts [37]. The CAp coatings did not show delamination either after the 10 week-immersion in a cell culture medium or after the osteoclast culture [37, 38].

The bioabsorption rate and the corrosion resistance of the CAp-coated Mg/Mg alloys should vary depending on the site and condition of the affected part of the body. The carbonate content can be utilized to control the bioabsorption rate of the CAp coatings

because the rate of osteoclastic resorption of CAp depends on the carbonate content [39]. Therefore, the carbonate content in the CAp coating needs to be controlled. A simple carbonate content measurement method would facilitate the control of the carbonate content in the CAp coatings and the quantitative evaluation of the corrosion and bioabsorption behaviors of the CAp-coated Mg/Mg alloys.

The carbonate content can be calculated from the coating composition obtained by surface analysis such as X-ray photoelectron spectroscopy (XPS), X-ray fluorescence (XRF), energy dispersive spectroscopy (EDS) and so on. The XPS analysis is suitable for deriving the carbonate content of the CAp coatings because, owing to the advantage of being able to analyze the chemical bonding state of the constituent elements, the carbonate groups in CAp can be distinguished from carbon in contaminating hydrocarbons, although only the composition of the outermost surface can be analyzed.

Meanwhile, the carbonate content of B-type CAp can be estimated from the position of apatite 002 plane X-ray diffraction (XRD) peak [31, 32] because the crystal lattice of apatite is extended in the c-axis direction in proportion to the substitution of the phosphate groups by carbonate groups [31, 40-42]. A proportionality constant for the relationship between the carbonate content and the 002-plane peak position was reported for CAp synthesized by precipitation method using $CaHPO_4$ and Na_2CO_3 solutions [31, 32]. Using this relationship, the carbon content of the CAp coatings of WE43 was roughly estimated to be 17-23wt% which is higher than the 7.4 wt% of human bone apatite [39]. However, it has not yet been investigated whether the existing empirically obtained proportionality constant can be applied to the CAp coatings formed on Mg/Mg alloys.

In this study, to utilize the carbon content to control the corrosion and bioabsorption behavior of the CAp-coated Mg/Mg alloys, the carbonate content of the CAp coatings

was varied by $NaHCO_3$ concentration of the coating solution, and the carbonate content was evaluated. The HAp and CAp coatings were formed on pure Mg in the coating treatment solutions with four different carbonate concentrations of 0, 0.25, 0.5 and 1.0 mol/L which is relatively lower than those for WE43 [39] to obtain the carbonate content comparable to those of bone apatite. The coating morphology was observed using scanning electron microscopy (SEM). The formation of apatite and the incorporation of carbonate groups in apatite were examined using XRD and Fourier transform infrared spectroscopy (FTIR). The coating composition, chemical state of carbonate groups, and carbonate content of the coatings were analyzed using XPS. The carbonate content values obtained by XPS measurements were compared with those estimated from XRD results using the existing proportionality constant, to examine the existing constant used for XRD results was appropriate.

2. Materials and methods

2.1 HAp and CAp coating of pure Mg

Pure Mg (99.5%, OSAKA FUJI) disks with a diameter of 15 mm and a thickness of 2 mm were prepared from extruded rods. The composition of pure Mg is shown in Table 1. The surface of disks was ground with SiC papers up to #1200 and rinsed ultrasonically in 2-propanol.

The HAp and CAp coatings were formed on pure Mg in a single step, simply by immersing in the following coating treatment solutions. The coating treatment solutions consisting of 0.2 mol/L calcium disodium ethylenediaminetetraacetate ($C_{10}H_{12}CaN_2Na_2O_8$, Ca-EDTA, Sigma), 0.2 mol/L potassium dihydrogen phosphate

(KH_2PO_4, Fujifilm-Wako), and 0, 0.25, 0.5, and 1.0 mol/L sodium hydrogen carbonate ($NaHCO_3$, Fujifilm-Wako) were prepared. The pH of the solutions was adjusted to 8−9 by adding an appropriate amount of 1 mol/L sodium hydroxide (NaOH, Fujifilm-Wako) solution. The solutions were heated to 363 K, and then as-polished pure Mg disks were immersed in the solution for 60 min. The coated disks were removed from the solution, rinsed with ultrapure water, and then dried at room temperature. The coated specimens were named HAp-Mg, CAp0.25-Mg, CAp0.5-Mg, and CAp1.0-Mg according to the $NaHCO_3$ concentrations in the coating solutions.

2.2 Characterization of HAp and CAp coatings

The surface and cross section of the HAp and CAp coatings were observed using SEM (JSM6500F, JEOL). The crystal structure was identified with XRD (Smart-Lab, RIGAKU) using Cu Kα radiation (λ=0.15406 nm), and the carbonate content of the HAp and CAp coatings was estimated from the position of the apatite 002 plane diffraction peak. Three samples were measured with XRD for each coated specimen to obtain the apatite 002 plane peak position. Incorporation of the carbonate groups in the apatite structure was examined with diffuse reflectance FTIR (IRTracer-100, Shimadzu) at 4 cm^{-1} resolution. The composition and the chemical state of constituent elements of the HAp and CAp coatings were analyzed with XPS (JPS-9010, JEOL) using Mg Kα radiation ($h\nu$=1253.6 eV). The pass energy was set to 50 eV for wide scan, 10 eV for narrow scan. The binding energies of all the spectra were referenced to the C 1s peak at 284.7 eV. The composition of three samples were quantified using XPS for each coated specimen, and then the carbonate content in the apatite was calculated.

3. Results and Discussion

3.1 Morphology of HAp and CAp coatings

Figure 1 shows the surface and cross-sectional SEM images of the HAp-Mg, CAp0.25-Mg, CAp0.5-Mg and CAp1.0-Mg specimens. The HAp coating shows a two-layer structure: a dense inner layer of 1 μm thick and an outer layer consisting of rod-shaped crystals about 1 μm long and 0.1 μm thick growing from the inner layer as reported previously [23]. The inner layer appears to consist of dome-shaped particles of about 1 μm agglomerated. The CAp0.25 coating consists of about 1 μm dome-shaped particles covered by about 0.1 μm particles. The CAp0.5 and CAp1.0 coatings show a cauliflower-like single layer consisting of dome-shaped particles as previously reported for the CAp coatings formed on WE43 with higher $NaHCO_3$ concentrations [37]. The size of dome-shaped particles decreases from about 1 to 0.5 μm with an increase in the $NaHCO_3$ concentration of the coating solutions. Assuming that one dome-shaped particle has grown from one crystal nucleus, the higher the $NaHCO_3$ concentration of the coating solution, the higher the frequency of apatite nucleation and the denser the coating. As the result, the thickness of the CAp coatings decreases from 2 to 1 μm with the $NaHCO_3$ concentration. LeGeros et al. reported that for CAp synthesized by precipitation method, the size of apatite crystals decreased with an increase in carbonate content. They interpretated this as being due to the carbonate ions forming weak bonds in the crystal structure and suppressing crystal growth in the direction of the weak bonds [40]. Such suppression of crystal growth by carbonate ions is presumed to cause the decrease in the size of dome shaped particles with the increase in $NaHCO_3$ concentration, thereby decreasing the coating thickness.

3.2 XRD patterns of HAp and CAp coatings

Figure 2(a) shows the wide-range raw XRD patterns of HAp-Mg, CAp0.25-Mg, CAp0.5-Mg and CAp1.0-Mg specimens. All the specimens show the diffraction peaks from pure Mg at 32.3, 34.5, 36.7, 47.9 and 57.5 degrees and those from apatite at around 26, 32.9 and 53 degrees. No peak other than Mg and apatite appeared, indicating that only apatite was formed in the HAp and CAp coatings.

The peaks at around 26, 32.9 and 53 degrees are derived from the 002, 300 and 004 planes of apatite (#00-009-0432), respectively. The small 300 plane peak at 32.9 degrees shows no change in peak position with the $NaHCO_3$ concentration as in the case for WE43 [37], indicating that hydroxyl groups were rarely substituted by carbonate groups.

Figure 2(b) shows the magnified diffraction peaks from 002 plane of the apatite after background processing and $K\alpha_2$ removal, and Fig. 2(c) shows the position of 002 plane peak as a function of the $NaHCO_3$ concentration. As the $NaHCO_3$ concentration increases from 0 to 0.5 mol/L, the position of 002 plane peak shifts from 25.87 degrees to 25.74 degrees, and becomes almost constant over 0.5 mol/L. The shift of the 002 plane peak position to the low angle side indicates that the crystal lattice of CAp is extended in the c-axis direction and that the B-type CAp, in which phosphate groups of apatite were substituted by carbonate groups, was formed [31, 40-42].

3.3 FTIR spectra of HAp and CAp coatings

Figure 3 shows the FTIR spectra of the HAp-Mg, CAp0.25-Mg, CAp0.5-Mg and CAp1.0-Mg specimens. The HAp-Mg exhibits a typical FTIR spectrum of HAp consisting of peaks at 550, 600, 960, 1010, 1085 and 1150 cm^{-1} derived from PO_4^{3-}, a peak around 870 cm^{-1} derived from HPO_4^{2-} and/or CO_3^{2-}, a broad peak around 3200 cm^{-1} derived from H_2O and very small peaks at 3550 and 3680 cm^{-1} derived from OH^- [31, 43-45] in addition to small peaks at 1650 and 1450 cm^{-1} derived from CO_3^{2-}. The HAp formed on WE43 also exhibited the similar FTIR spectrum [37]. The peak around 870 cm^{-1} is mainly attributed to CO_3^{2-} because of the appearance of CO_3^{2-}-derived peaks at 1650 and 1450 cm^{-1}. On the other hand, a part of the 870 cm^{-1} peak is attributed to HPO_4^{2-} because the OH^--derived peak at 3680 cm^{-1} is attributed to the OH stretching vibration of the surface P-OH group [46]. The appearance of the HPO_4^{2-} peak around 900 cm^{-1} is suggested to imply that the apatite is deficient in Ca^{2+} and contains H^+ in compensation for the Ca deficiency [47]. The Ca-deficient apatite was formed on Mg-3mass% RE-1mass% Y (EW31) and Mg-4mass% rare earth (RE4) of which the corrosion resistance was lower than WE43 and pure Mg [25], indicating that high concentration of Mg^{2+} ions dissolved from the substrate Mg alloy might be responsible for the formation of the Ca-deficient apatite. The 870 cm^{-1} peak of the HAp-Mg suggests that the HAp coating possibly contains the Ca-deficient apatite.

The CAp-Mg specimens exhibit peaks at 875, 1400, and 1470 cm^{-1}, which are derived from CO_3^{2-} in B-type CAp, in addition to the peaks derived from PO_4^{3-}, H_2O and OH^- groups of apatite [31, 43-45, 48]. Although the CO_3^{2-}-derived peak overlaps with the HPO_4^{2-}-derived peak around 900 cm^{-1}, the 875 cm^{-1} peak derived from CO_3^{2-} in B-type CAp is sharp and distinct in the CAp coatings. The presence of HPO_4^{2-} in the CAp coatings was therefore not determined only by the FTIR measurement. The intensity of

the absorption peaks at 550 and 600 cm^{-1} derived from PO_4^{3-} decreases with the increase in the $NaHCO_3$ concentration. These results confirm that carbonate groups are incorporated in apatite structure by substituting phosphate groups. In the absorption band from 950 to 1150 cm^{-1} derived from PO_4^{3-}, the relative intensity of the 1000 cm^{-1} peaks to the 955 cm^{-1} peak increases while the relative intensity of the 1150 cm^{-1} peak to the 955 cm^{-1} peak decreases with the $NaHCO_3$ concentration. This result indicates an environmental change around the phosphate groups in the apatite structure. However, the quantitative studies will be carried out in the future because the substance concentration and the IR absorption intensity often do not show a linear relationship in the diffuse reflectance method [49].

3.4 XPS spectra of HAp and CAp coatings

Figure 4 shows the XPS survey spectrum of the CAp0.25-Mg as typical for all the specimens. The survey spectrum shows clear peaks of Ca, P, O, C and Na and a tiny peak of Mg. It is considered that Ca, P, O, and a part of C are derived from the HAp and CAp coatings and most of C is derived from contamination. The Na 1s peak significantly decreased by Ar sputtering and Na is originated from Ca-EDTA ($(C_{10}H_{12}CaN_2Na_2O_8)$), indicating that Na was present as EDTA-Na or sodium phosphate on the outside of the HAp and CAp coating as in the case of the HAp-Mg treated for 2 h [50]. Since apatite has a high affinity for organic substances, EDTA could not be completely removed by lightly rinsing in pure water. Mg is considered to be derived from substrate pure Mg, the HAp and CAp coatings and $Mg(OH)_2$ formed at the boundary between substrate and coating [23].

Figure 5 shows the XPS spectra of C 1s electron of the HAp-Mg, CAp0.25-Mg, CAp0.5-Mg, and CAp1.0-Mg specimens. The C 1s peak of the HAp-coated specimen is decomposed into peaks at 284.7 and 288.5 eV while that of the CAp-coated specimens is decomposed into peaks at 284.7, around 288.5 and around 289.5 eV which are attributed to C-C bond and CO_3^{2-} and HCO_3^-, respectively [51]. The total intensity of the CO_3^{2-} and HCO_3^- peaks increases and the relative intensity of the HCO_3^- peak to the CO_3^{2-} peak ($I_{HCO_3^-}/I_{CO_3^{2-}}$) increases with the increase in the $NaHCO_3$ concentration. These results indicate that there are two types of carbonate group, CO_3^{2-} and HCO_3^-, in the apatite structure. Similar to the presence of HPO_4^{2-}, the presence of HCO_3^- presumably suggests the formation of Ca-deficient apatite.

Figure 6 shows the XPS spectra of the O 1s electron of the HAp- and CAp-coated specimens. The O 1 s peak is decomposed into peaks around 530.6, 531.4 and 532.5 eV which are attributed to O^{2-}, hydroxide or hydroxyl group (OH^-) and hydrate and/or adsorbed water (H_2O), respectively [52, 53]. According to the chemical formulas of $Ca_{10}(PO_4)_6(OH)_2$ for HAp and $Ca_{10-a}(PO_4)_{6-b}(CO_3)_c(OH)_{2-d}$ for CAp, the O^{2-} and OH^- are from the HAp and CAp coatings. The relative intensity of the OH^- peak to the O^{2-} peak of the CAp coatings is higher than that of the HAp coating. This result is consistent to the presence of HCO_3^- in the CAp coatings.

Figure 7 shows the XPS spectra of the P 2p electron of the HAp- and CAp-coated specimens. The P 2p peak is decomposed into two peaks at 132.2-132.5 eV and 133.2-133.4 eV which are attributed to PO_4^{3-} and HPO_4^{2-}, respectively [54]. This result is consistent to the result that the FTIR spectra show the absorption peaks from PO_4^{3-} and HPO_4^{2-}. The presence of HPO_4^{2-} is attributed mainly to the surface P-OH group which is indicated by the OH^--derived peak at 3680 cm^{-1} on the FTIR spectra (Fig. 3). In the same

time, the presence of HPO_4^{2-} was reported to suggest the formation of Ca-deficient apatite [47]. The relative intensity of the HPO_4^{2-} peak to the PO_4^{3-} peak appears to be higher for the CAp coating than for the HAp coatings, while there is no obvious difference in the intensity ratio of the PO_4^{3-} peak to the HPO_4^{2-} peak with the $NaHCO_3$ concentration. It was not found whether PO_4^{3-} or HPO_4^{2-} was preferentially substituted by carbonate groups. The FTIR measurements suggested the formation of the Ca-deficient apatite in the HAp coating, while it was not evident in the CAp coatings. However, the appearance of the HPO_4^{2-} peak as well as HCO_3^- peak in the XPS spectrum suggests that the CAp coatings also contain Ca-deficient apatite.

Figure 8 shows the XPS spectra of the Ca 2p and Mg 2p electrons of the HAp- and CAp-coated specimens. The binding energy of the Ca 2p3/2 peak of the HAp-Mg and CAp0.25-Mg is 346.4 eV and 346.8 eV, respectively and that of the CAp0.5-Mg and CAp1.0-Mg is 347.0 eV. These binding energies basically agree with the values for calcium phosphates [55]. Therefore, the difference in the binding energy of the Ca 2p peak between the HAp and the CAp coatings can be attributed to the substitution of phosphate groups in the apatite by carbonate groups.

The Mg 2p spectra are too small to discuss the precise chemical state. However, the binding energy of the Mg 2p peak is 50.2-50.4 eV, which corresponds to that of $Mg(OH)_2$ [56]. It was reported that $Mg(OH)_2$ was formed at the boundary between HAp coating and substrate pure Mg [23] and that small amount of Mg was incorporated into the HAp coating of the HAp-Mg treated for 2 h [56]. These facts indicate that Mg is derived from the apatite coatings and the $Mg(OH)_2$ at the boundary.

The content of carbonate and phosphate groups were calculated by the following equations (1) and (2), respectively.

$$x_{CO} = \frac{[CO_3^{2-}]+[HCO_3^-]}{[Ca^{2+}]+[Mg^{2+}]+[PO_4^{3-}]+[HPO_4^{2-}]+[CO_3^{2-}]+[HCO_3^-]+[OH^-]} \quad (1)$$

$$x_{PO} = \frac{[PO_4^{3-}]+[HPO_4^{2-}]}{[Ca^{2+}]+[Mg^{2+}]+[PO_4^{3-}]+[HPO_4^{2-}]+[CO_3^{2-}]+[HCO_3^-]+[OH^-]} \quad (2)$$

where x_{CO} and x_{PO} are the total carbonate and phosphate contents (at%), respectively, and [*C*] is the atomic fraction of the constituent of the HAp and CAp coating. Three samples were measured with XPS for each coated specimen. As it was considered that most of the detected Na was not incorporated in the apatite structure, Na was not included in the calculation of the carbonate and phosphate contents.

Figure 9 shows the atomic content of phosphate and carbonate groups as a function of the $NaHCO_3$ concentration of the coating solutions. The total phosphate content decreases while the total carbonate content increases with the increase in the $NaHCO_3$ concentration, according to the substitution of phosphate groups by carbonate groups. For the content of HCO_3^- and CO_3^{2-}, the CO_3^{2-} content increases between 0 and 0.5 mol/L $NaHCO_3$ and becomes almost constant above 0.5 mol/L $NaHCO_3$. The HCO_3^- content increases almost monotonically with the increase in the $NaHCO_3$ concentration. At 0 mol/L $NaHCO_3$, the CO_3^{2-} content is higher than the HCO_3^- content in the HAp coating. As the HCO_3^- content increases and the CO_3^{2-} content is almost constant with the $NaHCO_3$ concentration, the HCO_3^- content becomes higher than the CO_3^{2-} content in the CAp coating formed with 1.0 mol/L $NaHCO_3$. These results suggest that the environment around the carbonate groups changes when the $NaHCO_3$ concentration exceeds 0.5 mol/L. Since the presence of HPO_4^{2-} is attributed to the surface P-OH group [46] and the

formation of Ca deficient apatite [47], the presence of HCO_3^- also suggests the presence of surface C-OH group and the Ca deficient in apatite structure.

3.5 Carbonate content of HAp and CAp coatings derived by XRD and XPS measurements

Figure 10 shows the carbonate content obtained by XRD and XPS measurements as a function of the $NaHCO_3$ concentration in the coating solutions. In the case of the XRD measurements, the carbonate content of the apatite coatings was estimated from the c-axis length of the crystal lattice obtained from the apatite 002 peak position using equation (3) [31, 32].

$$l_c = 0.002145 \times w_C(wt\%) + \alpha \quad (3)$$

where l_c is the c-axis length (Å), w_C is carbonate weight content (wt%) and α is the c-axis length of hydroxyapatites with stoichiometric composition. The proportionality constant of 0.002145 was empirically obtained using CAp synthesized in the solution of different composition [31, 32]. For the carbonate content calculated from the XPS results, the atomic content shown in Fig. 9 was converted to the weight content. As shown in Fig. 10, the carbonate contents obtained from the XPS and XRD results are in good accordance, indicating that the obtained values are reliable. Also, it is confirmed that the carbon content of the CAp coatings formed on pure Mg can be estimated with sufficient

reliability from the XRD peak position of apatite 002 plane using Eq. (3), which includes the empirically obtained proportionality constant.

The HAp-Mg shows the carbonate content of about 2wt%, which is attributed to the dissolution of CO_2 from the air into the coating solution. The carbonate content of the CAp0.25-Mg, CAp0.5-Mg and CAp1.0-Mg is about 12, 15 and 18wt%, respectively. These values are in the carbonate content range of bone apatite of 7.4-20wt% [39], indicating that the CAp coatings can be resorbed by osteoclast cells in the same manner as bone.

In our previous study, the carbonate content of the CAp0.4M, CAp1.1M and CAp1.9M coatings of WE43 was estimated to be about 17, 29 and 23wt%, respectively, from the XRD peak position of apatite 002 plane [37], which are plotted in Fig. 10 as a comparison. The carbonate content of the CAp coatings formed on pure Mg shows good consistency with that of the CAp coatings formed on WE43. It was eventually revealed that the carbonate content in the CAp coatings does not depend on the substrate Mg/Mg alloys, and the carbonate content can be determined solely by XRD measurements. Also, it was demonstrated that it can be varied between 2 and 23wt% by the $NaHCO_3$ concentration in the coating solution.

4. Conclusions

The HAp and CAp coatings with different carbonate contents were formed on pure Mg using the aqueous coating solutions with different $NaHCO_3$ concentrations of 0, 0.25, 0.5 and 1.0 mol/L. The formation of HAp and CAp was confirmed by XRD and FTIR measurements. The carbonate content of the HAp and CAp coatings was derived in two

methods: the estimation from the XRD peak position of the apatite 002 plane using the existing empirically obtained proportionality constant and the quantitative analysis with XPS. The findings are summarized as follows:

1. The carbonate content of the HAp and B-type CAp coatings formed with 0, 0.25, 0.5 and 1.0 mol/L $NaHCO_3$ was determined to be 2, 12, 15 and 18wt%, respectively, from the XRD and XPS measurements. The carbonate content of the CAp coatings of Mg/Mg alloys can be precisely controlled in the comparable range as those of bone apatite by the $NaHCO_3$ concentration in the coating solution.

2. The carbonate content of the HAp and B-type CAp coatings derived from the XRD peak position of apatite 002 plane using the existing proportionality constant was in good accordance with that calculated from the composition quantified by the XPS measurements. The carbonate content of the B-type CAp coatings can be accurately determined from the position of the apatite 002 plane XRD peak using the existing proportionality constant.

3. Two types of carbonate group, CO_3^{2-} and HCO_3^-, were present in the CAp coatings. The relative content of HCO_3^- to CO_3^{2-} increased with the increase in the $NaHCO_3$ concentration of the coating solution.

Author contribution

K. Midorikawa carried out experiments and analyzed data. S. Hiromoto designed research plan, analyzed data and wrote the paper. T. Yamamoto contributed to analyze XPS data.

Acknowledgements

This work was partially supported by JSPS KAKENHI Grant Number [19H02449, 22H01798] and by the Light Metal Educational Foundation. The FTIR measurement was supported by the NIMS Molecule & Material Synthesis Platform in the Nanotechnology Platform Project. XRD and XPS measurements were carried out at Kagami Memorial Research Institute for Materials Science and Technology, Waseda University.

Declaration of competing interest

The authors declare that they have no known competing financial interests or personal relationships that could have appeared to influence the work reported in this paper.

Data availability

The raw/processed data required to reproduce these findings cannot be shared at this time as the data also form part of an ongoing study.

References

[1] F. Witte, N. Hort, C. Vogt, S. Cohen, K.U. Kainer, R. Willumeit, F. Feyerabend, Curr. Opin. Solid State Mater. Sci., 12 (2008) 63-72. 10.1016/j.cossms.2009.04.001

[2] R.C. Zeng, W. Dietzel, F. Witte, N. Hort, C. Blawert, Adv. Biomater., 10 (2008) B3-B14. 10. 1002/adem.200800035

[3] D.W. Zhao, F. Witte, F.Q. Lu, J.L. Wang, J.L. Li, L. Qin, Biomaterials, 112 (2017) 287-302. 10.1016/j.biomaterials.2016.10.017

[4] H.S. Han, S. Loffredo, I. Jun, J. Edwards, Y.C. Kim, H.K. Seok, F. Witte, D. Mantovani, S. Glyn-Jones, Materials Today, 23 (2019) 57-71. 10.1016/j.mattod.2018.05.018

[5] M. Baldini, V. Coppa, D. Falcioni, E. Senigagliesi, M. Marinelli, A.P. Gigante, J Child Orthop, 15 (2021) 194-203. 10.1302/1863-2548.15.210004

[6] C. Plaass, S. Ettinger, L. Sonnow, S. Koenneker, Y. Noll, A. Weizbauer, J. Reifenrath, L. Claassen, K. Daniilidis, C. Stukenborg-Colsman, H. Windhagen, J. Orthop. Res., 34 (2016) 2207-2214. 10.1002/jor.23241

[7] M. Joner, P. Ruppelt, P. Zumstein, C. Lapointe-Corriveau, G. Leclerc, A. Bulin, M.I. Castellanos, E. Wittchow, M. Haude, R. Waksman, EuroIntervention, 14 (2018) e1040-e1048. 10.4244/EIJ-D-17-00708

[8] C. Sukotjo, T.J. Lima-Neto, J.F. Santiago Junior, L.P. Faverani, M. Miloro, Materials (Basel), 13 (2020) 3914. 10.3390/ma13183914

[9] R. Waksman, P. Zumstein, M. Pritsch, E. Wittchow, M. Haude, C. Lapointe-Corriveau, G. Leclerc, M. Joner, EuroIntervention, 13 (2017) 440-449. 10.4244/EIJ-D-16-00915

[10] Y. Al-Abdullat, S. Tsutsumi, N. Nakajima, M. Ohta, H. Kuwahara, K. Ikeuchi, Mater. Trans., 42 (2001) 1777-1780. 10.2320/matertrans.42.1777

[11] H. Kuwahara, Y. Al-Abdullat, N. Mazaki, S. Tsutsumi, T. Aizawa, Mater. Trans., 42 (2001) 1317-1321. 10.2320/matertrans.42.1317

[12] C.L. Wen, S.K. Guan, L. Peng, C.X. Ren, X. Wang, Z.H. Hu, Appl. Surf. Sci., 255 (2009) 6433-6438. 10.1016/j.apsusc.2008.09.078

[13] H. Hornberger, S. Virtanen, A.R. Boccaccini, Acta Biomater., 8 (2012) 2442-2455. 10.1016/j.actbio.2012.04.012

[14] S. Cheng, W. Wang, D. Wang, B. Li, J. Zhou, D. Zhang, L. Liu, F. Peng, X. Liu, Y. Zhang, Biomater. Sci., 8 (2020) 3320-3333. 10.1039/d0bm00467g

[15] J. Lou, Y. Sun, Y.D. Chen, R. Zan, H.Z. Peng, S. Yang, X.B. Kang, Z.X. Peng, W.H. Wang, X.N. Zhang, Surf. Coat. Tech., 422 (2021) 127552. ARTN 127552 10.1016/j.surfcoat.2021.127552

[16] H. Naujokat, C.B. Ruff, T. Kluter, J.M. Seitz, Y. Acil, J. Wiltfang, Int. J. Oral Maxillofac. Surg., 49 (2020) 272-283. 10.1016/j.ijom.2019.03.966

[17] Z.P. Kacarevic, P. Rider, A. Elad, D. Tadic, D. Rothamel, G. Sauer, F. Bornert, P. Windisch, D.B. Hangyasi, B. Molnar, T. Kammerer, B. Hesse, E. Bortel, M. Bartosch, F. Witte, Bioact. Mater., 14 (2022) 15-30. 10.1016/j.bioactmat.2021.10.036

[18] M. Fosca, A. Streza, I.V. Antoniac, G. Vadala, J.V. Rau, J. Funct. Biomater., 14 (2023). 10.3390/jfb14050250

[19] S.M. Kim, J.H. Jo, S.M. Lee, M.H. Kang, H.E. Kim, Y. Estrin, J.H. Lee, J.W. Lee, Y.H. Koh, J. Biomed. Mater. Res. A, 102A (2014) 429-441. 10.1002/jbm.a.34718

[20] F. Geng, L.L. Tan, X.X. Jin, J.Y. Yang, K. Yang, J. Mater. Sci.-Mater. Medic., 20 (2009) 1149-1157.

[21] S. Hiromoto, Electrochim. Acta, 54 (2009) 7085-7093. 10.1016/j.electacta.2009.07.033

[22] S. Hiromoto, M. Inoue, T. Taguchi, M. Yamane, N. Ohtsu, Acta Biomater., 11 (2015) 520-530. 10.1016/j.actbio.2014.09.026

[23] M. Tomozawa, S. Hiromoto, Acta Mater., 59 (2011) 355-363. 10.1016/j.actamat.2010.09.041

[24] M. Tomozawa, S. Hiromoto, Y. Harada, Surf. Coat. Tech., 204 (2010) 3243-3247. 10.1016/j.surfcoat.2010.03.023

[25] S. Hiromoto, E. Nozoe, K. Hanada, T. Yoshimura, K. Shima, T. Kibe, N. Nakamura, K. Doi, Mater. Sci. Eng. C-Mater. Biolog. Appl., 122 (2021) 111942. 10.1016/j.msec.2021.111942

[26] T. Kasuga, Coatings for metallic biomaterials, in: M. Niinomi (Ed.) Metals for biomedical devices, Woodhead Publishing Limited, Camridge(UK), 2010, pp. 260-282.

[27] Y. Doi, T. Shibutani, Y. Moriwaki, T. Kajimoto, Y. Iwayama, J. Biomed. Mater. Res., 39 (1998) 603-610. 10.1002/(Sici)1097-4636(19980315)39:4<603::Aid-Jbm15>3.3.Co;2-8

[28] K. Ishikawa, Materials, 3 (2010) 1138-1155. 10.3390/ma3021138

[29] M. Kanazawa, K. Tsuru, N. Fukuda, Y. Sakemi, Y. Nakashima, K. Ishikawa, J. Mater. Sci. Mater. Med., 28 (2017) 85. 10.1007/s10856-017-5896-5

[30] K. Ishikawa, Japanese Mag. Mineral. Petrol. Sci. 46 (2017) 42-46. 10.2465/gkk.161217

[31] R.Z. LeGeros, M.S. Tung, Caries Res., 17 (1983) 419-429. 10.1159/000260696

[32] M. Ohtsuka, Y. Matsuda, J. Assoc. Mater. Eng. Resourc., 4 (1991) 128-141. https://doi.org/10.5188/jsmerj.4.2_128

[33] T. Kokubo, F. Miyaji, H.-M. Kim, J. Am. Ceram. Soc., 79 (1996) 1127-1129. 10.1111/j.1151-2916.1996.tb08561.x

[34] L. Muller, E. Conforto, D. Caillard, F.A. Muller, Biomol. Eng., 24 (2007) 462-466. 10.1016/j.bioeng.2007.07.011

[35] T. Kokubo, S. Ito, Z.T. Huang, T. Hayashi, S. Sakka, T. Kitsugi, T. Yamamuro, J. Biomed. Mater. Res., 24 (1990) 331-343. 10.1002/jbm.820240306

[36] F. Barrere, C.M. van der Valk, R.A. Dalmeijer, C.A. van Blitterswijk, K. de Groot, P. Layrolle, J. Biomed. Mater. Res. A, 64 (2003) 378-387. 10.1002/jbm.a.10291

[37] S. Hiromoto, S. Itoh, N. Noda, T. Yamazaki, H. Katayama, T. Akashi, Sci. Tech. Adv. Mater., 21 (2020) 346–358. 10.1080/14686996.2020.1761237

[38] S. Hiromoto, S. Itoh, K. Doi, H. Katayama, T. Akashi, Corros. Sci., 200 (2022) 110222. 10.1016/j.corsci.2022.110222

[39] K. Ishikawa, Jinko Zoki, 47 (2018) 189-195. 10.11392/jsao.47.189

[40] R.Z. LeGeros, O.R. Trautz, J.P. Legeros, E. Klein, W.P. Shirra, Science, 155 (1967) 1409-1411. 10.1126/science.155.3768.1409

[41] R. Zapanta-LeGeros, Nature, 206 (1965) 403-404. 10.1038/206403a0

[42] Y. Suetsugu, Inorg. Mater., 3 (1996) 48-54. 10.11451/mukimate1994.3.48

[43] I. Rehman, W. Bonfield, J. Mater. Sci. Mater. Med., 8 (1997) 1-4. 10.1023/a:1018570213546

[44] S.A. Hutchens, R.S. Benson, B.R. Evans, H.M. O'Neill, C.J. Rawn, Biomaterials, 27 (2006) 4661-4670. 10.1016/j.biomaterials.2006.04.032

[45] D. Kuroda, M. Moriyama, R. Ichino, M. Okido, A. Seki, J. Japan Inst. Metals, 73 (2009) 346-353. 10.2320/jinstmet.73.346

[46] H. Tanaka, J. Soc. Powder Technol, 41 (2004) 369-377. 10.4164/sptj.41.369

[47] H. Aoki, Physical and Chemical Properties of Apatite, Amazing Biomaterials Apatite, Ishiyaku Publishers, Inc., Tokyo, 1999, pp. p.68-86,.

[48] Y. Suetsugu, J. Tanaka, J.Mater. Sci. Mater. Med., 10 (1999) 561-566. 10.1023/a:1008972432076

[49] S. Ochiai, Diffuse Reflection Measurements, in: M. Tasumi (Ed.) Experimental Infrared Spectroscopy - Fundamentals and Practical Methods, S.T.Japan Inc., Tokyo, 2012, pp. 79-83.

[50] N. Ohtsu, S. Hiromoto, M. Yamane, K. Satoh, M. Tomozawa, Surf. Coat. Tech., 218 (2013) 114-118. 10.1016/j.surfcoat.2012.12.037

[51] J.B. Abreu, J.E. Soto, A. Ashley-Facey, M.P. Soriaga, J.F. Garst, J.L. Stickney, J. Colloid Interface Sci., 206 (1998) 247-251. 10.1006/jcis.1998.5681

[52] K. Asami, K. Hashimoto, Corros. Sci., 17 (1977) 559-570. 10.1016/S0010-938x(77)80002-4

[53] S. Hiromoto, T. Hanawa, K. Asami, Biomaterials, 25 (2004) 979-986. 10.1016/s0142-9612(03)00620-3

[54] M. Tsunakawa, Y. Shimada, K. Nakamura, K. Kikuchi, T. Matsumura, T. Ishizaki, J. Jpn Inst. Light Metal., 67 (2017) 497–502. 10.2464/jilm.67.497

[55] N. Ohtsu, N. Masahashi, Y. Mizukoshi, Appl. Surf. Sci., 258 (2012) 6052-6055. 10.1016/j.apsusc.2012.02.132

[56] V. Fournier, P. Marcus, I. Olefjord, Surf. Interface Anal., 34 (2002) 494-497. 10.1002/sia.1346

Caption list

Table 1 Chemical composition of pure Mg used in this study (wt.%).

Fig. 1. (a)–(d) Surface and (e)–(h) cross-sectional SEM images of pure Mg specimens treated with $NaHCO_3$ concentrations of (a, e) 0 mol/L (HAp), (b, f) 0.25 mol/L (CAp0.25), (c, g) 0.5 mol/L (CAp0.5) and (d, h) 1.0 mol/L (CAp1.0).

Fig. 2. (a), (b) XRD patterns of pure Mg specimens treated in solutions with $NaHCO_3$ concentrations of 0, 0.25, 0.5 and 1.0 mol/L. (a) Wide range and (b) narrow range for apatite 002 plane (c-plane). (c) position of apatite 002 plane peak as a function of $NaHCO_3$ concentration of coating solution.

Fig. 3. FTIR absorption spectra of pure Mg specimens treated in coating solutions with 0, 0.25, 0.5 and 1.0 mol/L $NaHCO_3$. Spectra are vertically offset for clarity.

Fig. 4. XPS survey spectrum of CAp0.25-Mg.

Fig. 5. XPS narrow spectra of C 1s electron of (a) HAp-Mg, (b) CAp0.25-Mg, (c) CAp0.5-Mg, and (d) CAp1.0-Mg.

Fig. 6. XPS narrow spectra of O 1s electron of (a) HAp-Mg, (b) CAp0.25-Mg, (c) CAp0.5-Mg, and (d) CAp1.0-Mg.

Fig. 7. XPS narrow spectra of P 2p electron of of (a) HAp-Mg, (b) CAp0.25-Mg, (c) CAp0.5-Mg, and (d) CAp1.0-Mg.

Fig. 8. XPS narrow spectra of (a) Ca 2p and (b) Mg 2p electrons of HAp-Mg, CAp0.25-Mg, CAp0.5-Mg, and CAp1.0-Mg.

Fig. 9. Total phosphate group and total carbonate group content as well as CO_3^{2-} and HCO_3^- content obtained by XPS analysis as a function of $NaHCO_3$ concentration in the coating solutions.

Fig. 10. Total carbonate content of HAp-Mg and CAp-Mg specimens obtained by XRD and XPS analysis as a function of $NaHCO_3$ concentration in the coating solutions. The carbonate content of HAp-WE43 and CAp-WE43 specimens obtained by XRD measuremnts is cited from ref. [37].

Table 1 Chemical composition of pure Mg (wt.%).

Material	Fe	Si	Ni	Cu	Al	Mn	Cl	Pb	Zn	Mg
Pure Mg	0.0023	0.005	0.0002	0.0002	0.0049	0.0063	0.002	0.001	0.0055	Bal.

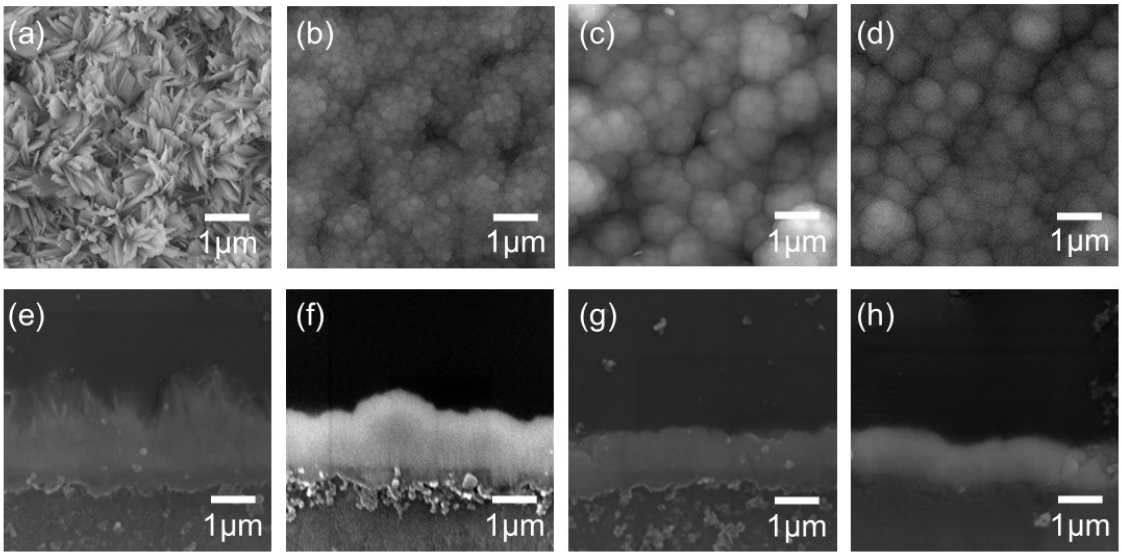

Fig. 1. (a)–(d) Surface and (e)–(h) cross-sectional SEM images of pure Mg specimens treated with $NaHCO_3$ concentrations of (a, e) 0 mol/L (HAp), (b, f) 0.25 mol/L (CAp0.25), (c, g) 0.5 mol/L (CAp0.5) and (d, h) 1.0 mol/L (CAp1.0).

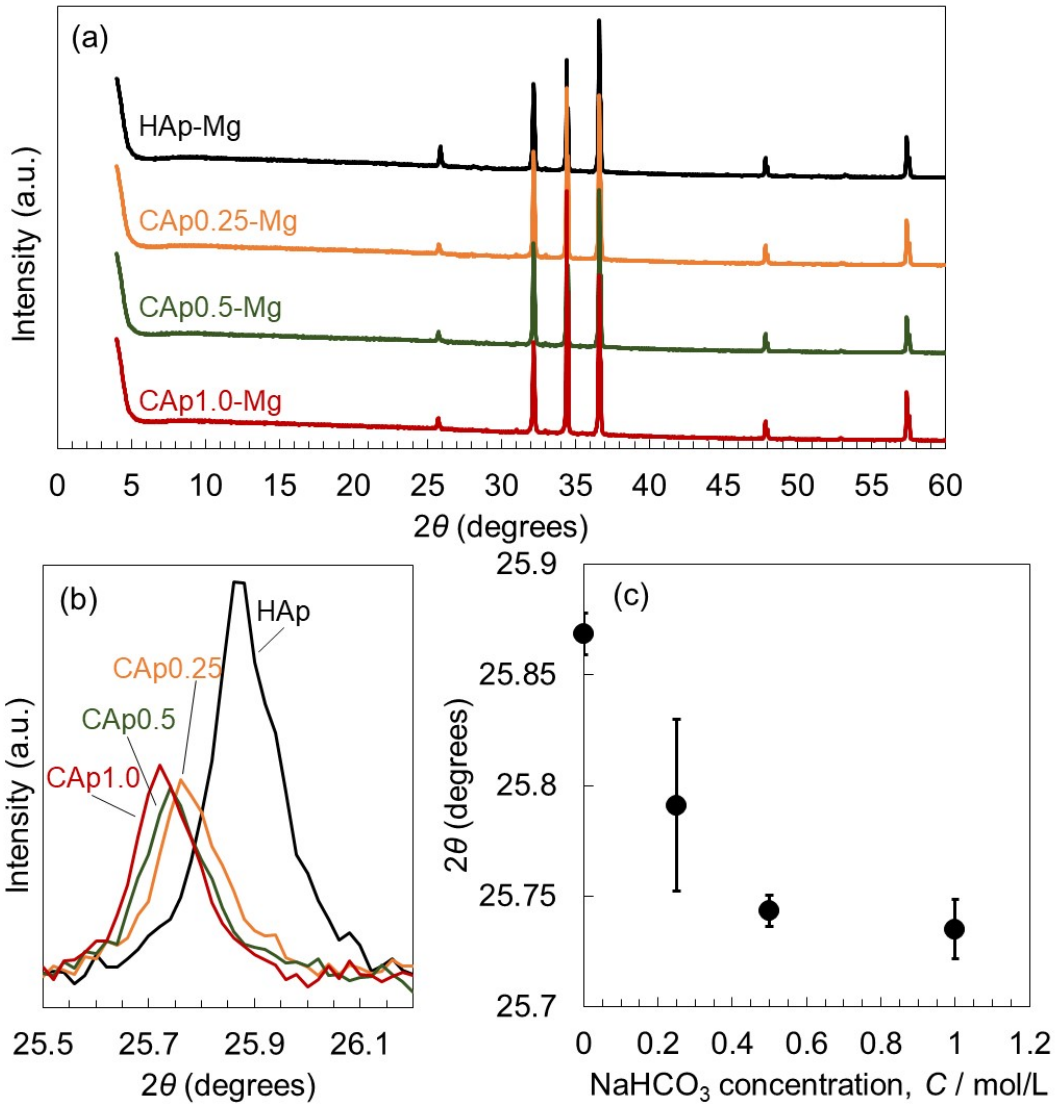

Fig. 2. (a), (b) XRD patterns of pure Mg specimens treated in solutions with $NaHCO_3$ concentrations of 0, 0.25, 0.5 and 1.0 mol/L. (a) Wide range and (b) narrow range for apatite 002 plane (c-plane). (c) position of apatite 002 plane peak as a function of $NaHCO_3$ concentration of coating solution.

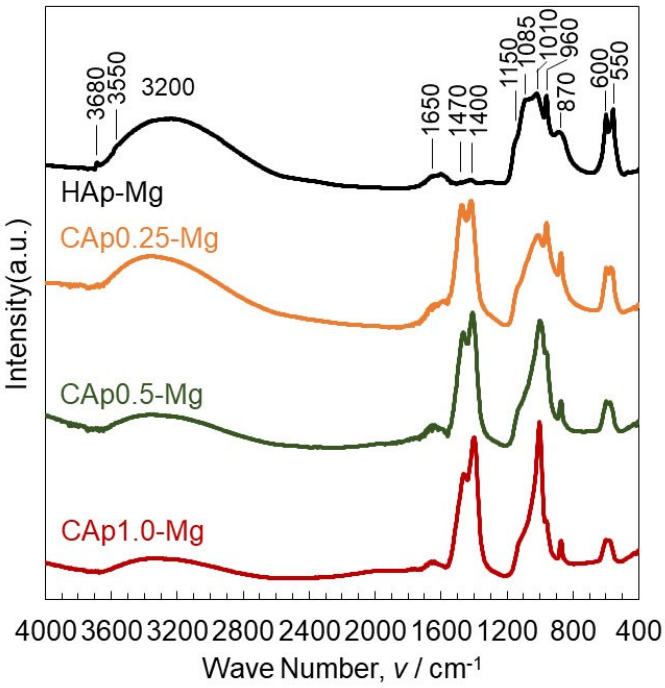

Fig. 3. FTIR absorption spectra of pure Mg specimens treated in coating solutions with 0, 0.25, 0.5 and 1.0 mol/L $NaHCO_3$. Spectra are vertically offset for clarity.

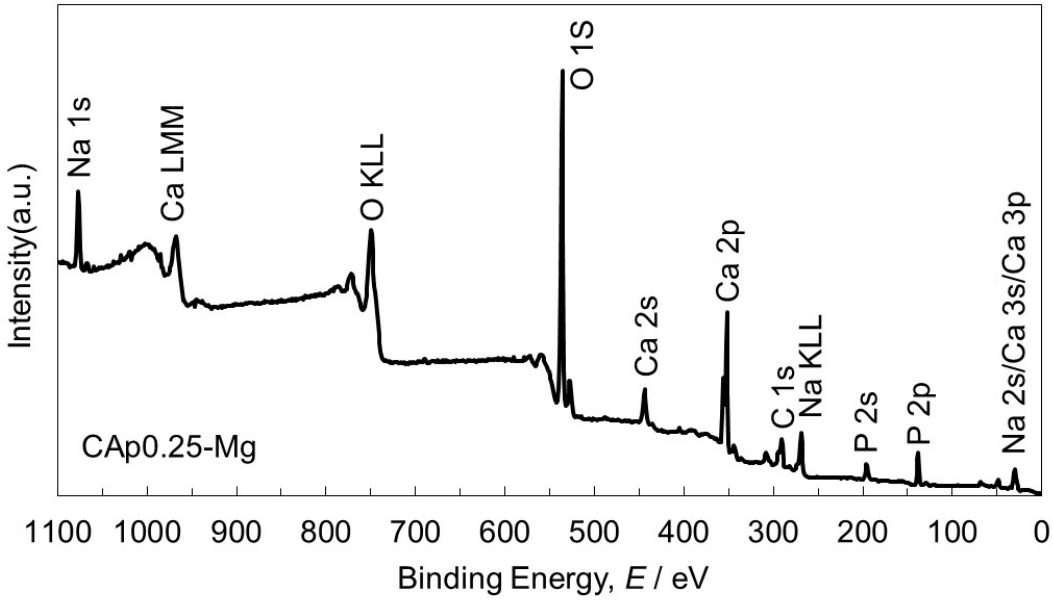

Fig. 4. XPS survey spectrum of CAp0.25-Mg.

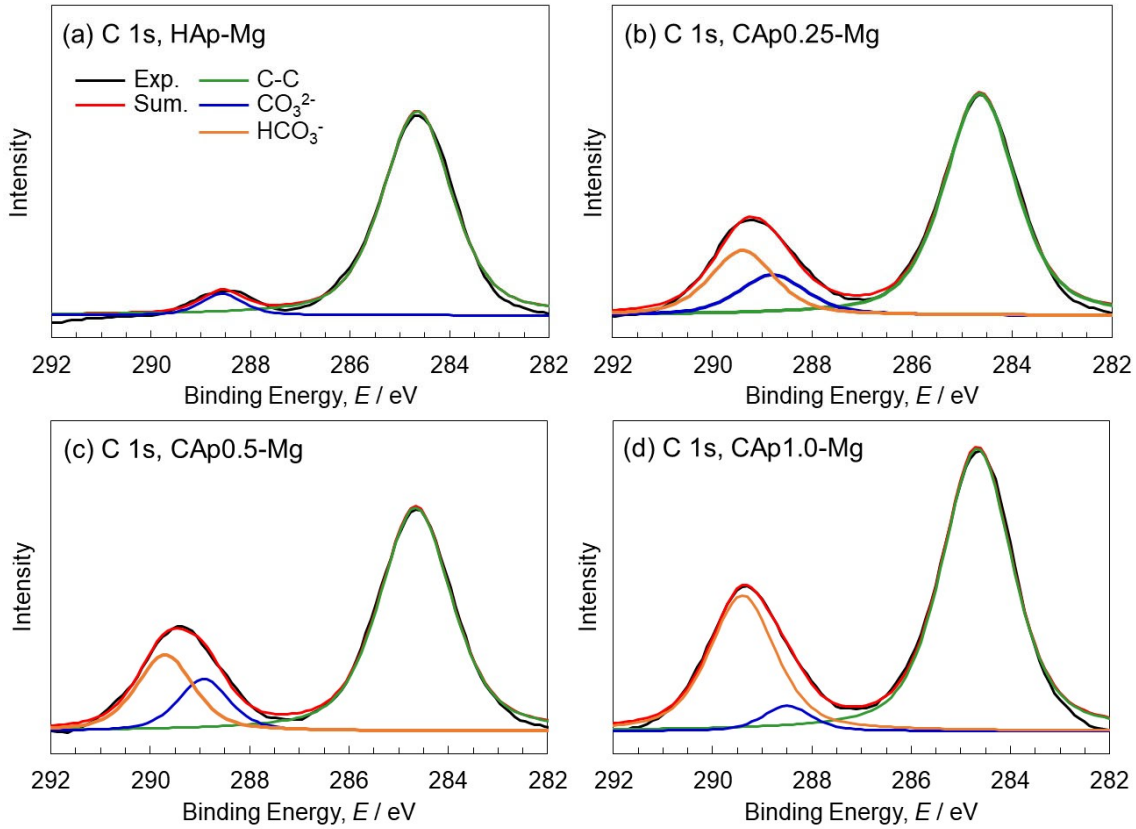

Fig. 5. XPS narrow spectra of C 1s electron of (a) HAp-Mg, (b) CAp0.25-Mg, (c) CAp0.5-Mg, and (d) CAp1.0-Mg.

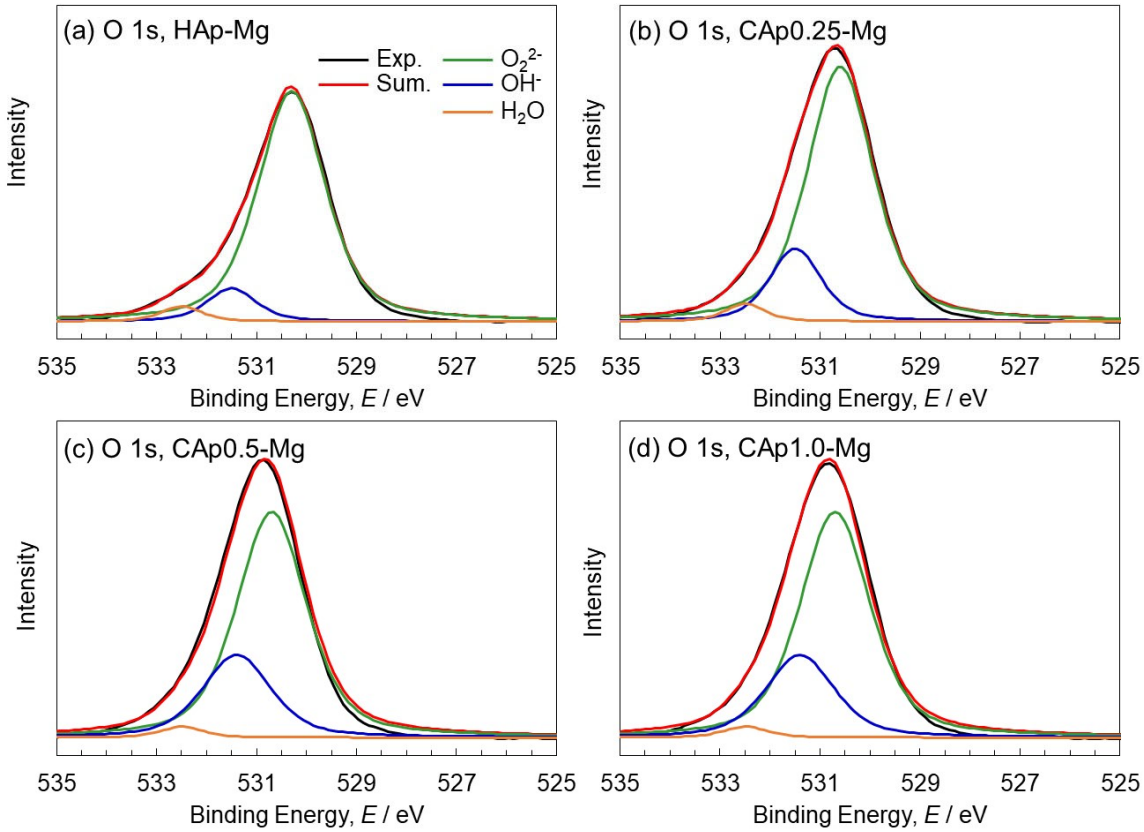

Fig. 6. XPS narrow spectra of O 1s electron of (a) HAp-Mg, (b) CAp0.25-Mg, (c) CAp0.5-Mg, and (d) CAp1.0-Mg.

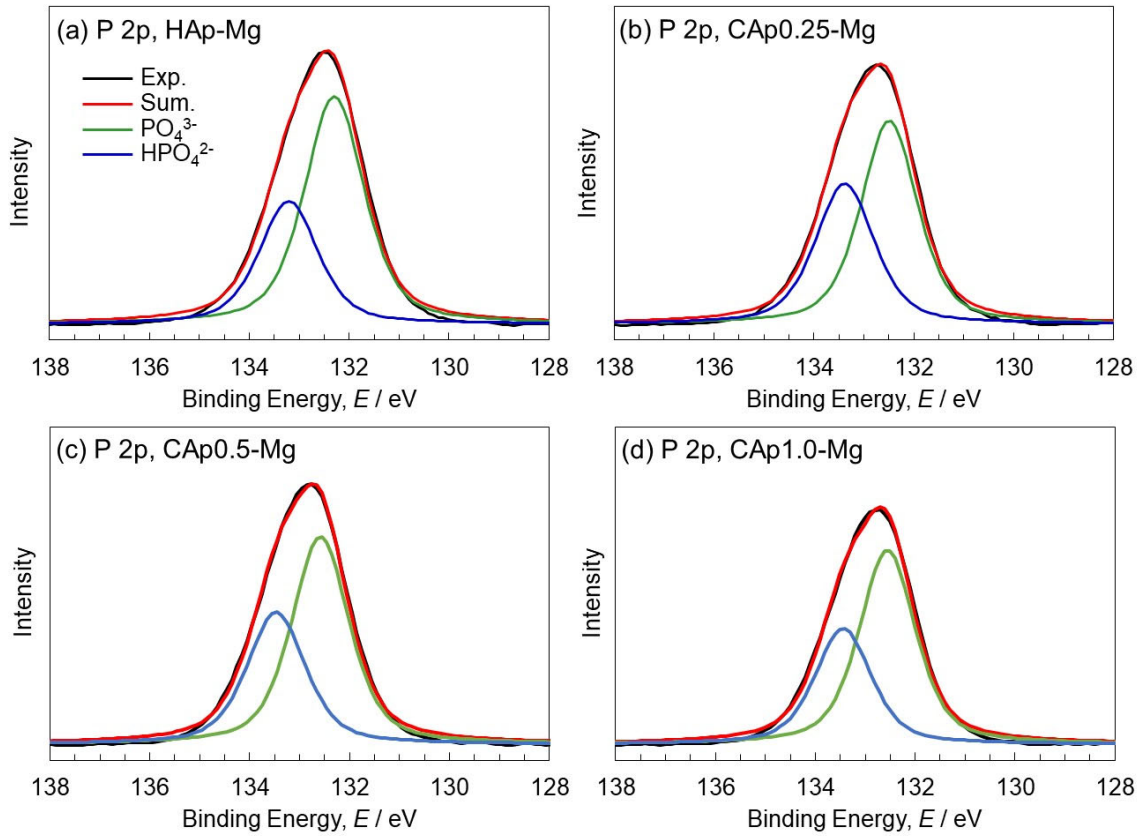

Fig. 7. XPS narrow spectra of P 2p electron of of (a) HAp-Mg, (b) CAp0.25-Mg, (c) CAp0.5-Mg, and (d) CAp1.0-Mg.

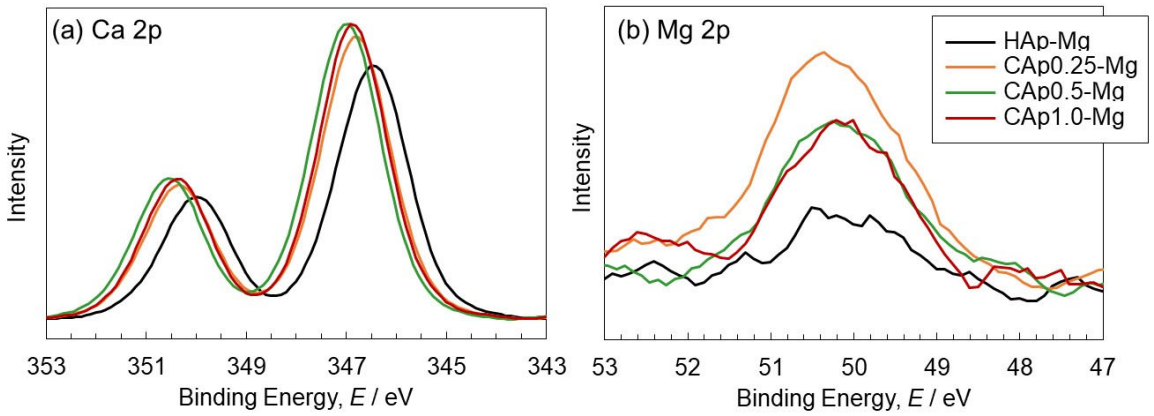

Fig. 8. XPS narrow spectra of (a) Ca 2p and (b) Mg 2p electrons of HAp-Mg, CAp0.25-Mg, CAp0.5-Mg, and CAp1.0-Mg.

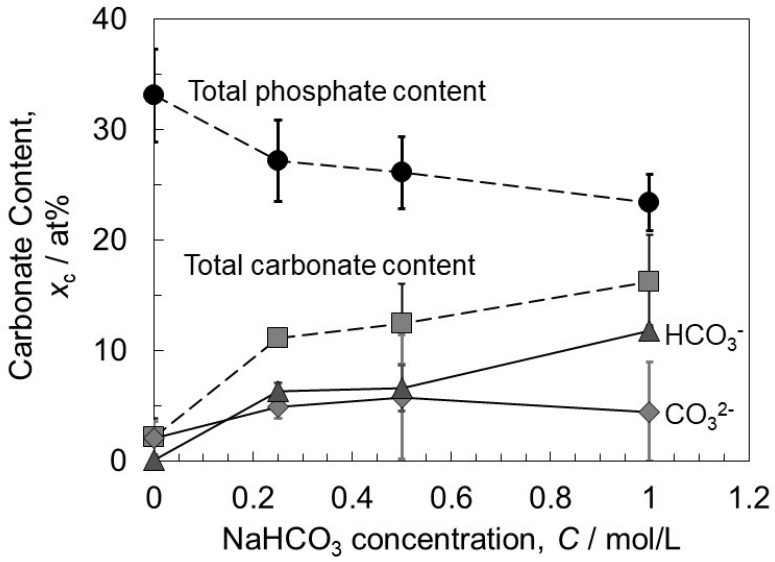

Fig. 9. Total phosphate group and total carbonate group content as well as CO_3^{2-} and HCO_3^- content obtained by XPS analysis as a function of $NaHCO_3$ concentration in the coating solutions.

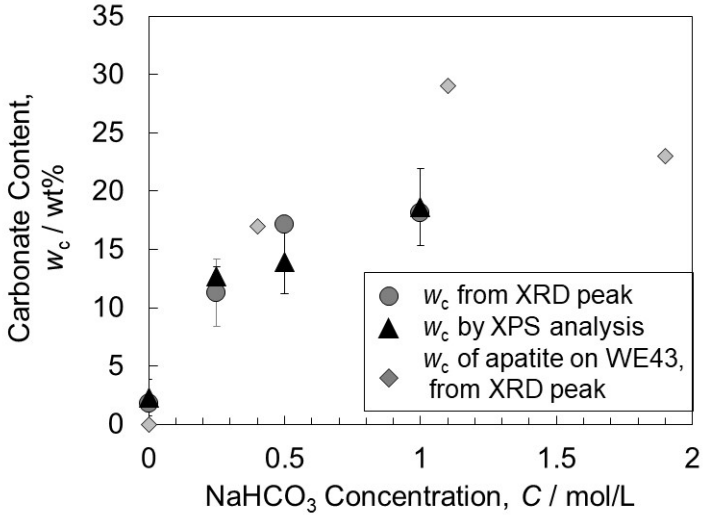

Fig. 10. Total carbonate content of HAp-Mg and CAp-Mg specimens obtained by XRD and XPS analysis as a function of $NaHCO_3$ concentration in the coating solutions. The carbonate content of HAp-WE43 and CAp-WE43 specimens obtained by XRD measuremnts is cited from ref. [37].